In-situ Observation of Slag Penetration into MgO Refractory

Kusuhiro Mukai*, Zainan Tao**, Kiyoshi Goto***, Zushu Li* and Toshiyasu Takashima****

*Faculty of Engineering, Kyushu Institute of Technology. 1-1 Sensui-cho, Tobata-ku, Kitakyushu 804-8550. **Fuji Finetec Co., Ltd., 2-10-11 Ano, Yahatanishi-ku, Kitakyushu 806-0049. ***Refractory Ceramics R&D Division, Steel Research Laboratories, Nippon Steel Corporation, 20-1 Shintomi, Futsu-shi, Chiba-ken 293-8511. ****Technical Research Center, Kurosaki Corporation, 1-1 Higashihama-machi, Yahatanishi-ku, Kitakyushu 806-8586.

ABSTRACT

The behavior of slag penetration into MgO refractory was investigated by combining *in-situ* X-ray observation with microstructural analysis of the samples after penetration experiments. The following results are obtained: The slag penetrates rapidly into the refractory, reacting with MgO particles in the refractory. The slag penetrates unevenly into the refractory with uneven pore size in a route like a tree, firstly along the main route (the surface of large MgO particles), and then extending to the branch route, while evenly into the refractory with even pore size. The rate of slag penetration increases with increasing pore radius and apparent porosity of the refractory, T.Fe concentration in the slag and temperature, and with decreasing the slag basicity (C/S ratio). In the case of the Al_2O_3-bearing slag, the rate of slag penetration is less than that of Al_2O_3-free slag in the initial stage. The penetration also stops much earlier than that of the Al_2O_3-free slag, and then the penetration height keeps almost constant. In the initial stage of penetration, the penetration height is proportional to the square root of penetration time. Slag penetration is deduced to stop due to the followings: 1) The melting point and viscosity of the penetrated slag increase, and the surface tension of the penetrated slag decreases with decreasing the Fe_tO concentration in the penetrated slag consumed by the reaction between Fe_tO and MgO particles. 2) In the 10mass%Al_2O_3-bearing slag, the pore size in the refractory is reduced by the spinel formed on the pore surface by the reaction between Al_2O_3 in the penetrated slag and MgO particles in the refractory.

KEYWORDS Slag penetration; Penetration rate; MgO refractory; X-ray radiographic technique; *In-situ* observation; Microstructural analysis.

1 Introduction

The slag penetration into refractory has a great influence on the corrosion of the refractory for changing the bonding between the composed particles in the refractory. Based on the analysis of the cooled samples after penetration experiments, some researchers have studied the slag penetration into refractory from some aspects such as the phase equilibrium of the components in the penetrated slag[1)] and the penetration rate of the slag[2)]. However, the *in-situ* observation of slag penetration and the study on the relationship between the slag penetration and the refractory microstructure are not reported until now.

In this research, the slag penetration into MgO refractory samples with different microstructure was directly observed with the X-ray radiographic technique. The behavior of the penetrated slag and the relationship between the slag penetration and the refractory microstructure were investigated by analyzing the cooled samples after penetration experiments.

2 Experimental

2.1 *In-situ* observation of slag penetration

Experiments were carried out in an electric resistance furnace with the X-ray radiographic apparatus as shown in Fig.1 at 1593K, 1693K and 1793K under an argon atmosphere at the

flow rate of 60~70ml/min.

Synthetic slag used in the experiments was made from chemical reagents of SiO_2 (first grade), Al_2O_3 (special grade), $CaCO_3$ (first grade) and FeO (purity $\geqq$92mass%). The chemical compositions of the slags are shown in Table 1. Three kinds of MgO refractories with different apparent porosity (Table 2) were used as samples in the experiments. In order to prevent the molten slag from creeping up along the sample surface, platinum wire (ϕ 0.9mm) was wound on the sample surface at the height of 2~3mm from the bottom of the sample. Pore size distribution in sample A and B measured by the mercury porosimetry is shown in Fig.2. In the sample A, the pores with the diameter of >10 μm amount to above 70%, and the pores with the diameter of >100 μm are rarely contained. In the sample B, the pores with the diameter of >100 μm amount to above 40%, and almost all the pores are above 10 μm in the diameter. As a whole, the pore size in the sample B is larger than that in the sample A, and its distribution in the sample B is also sharper (even-distributed) than that in the sample A. Uneven pore size in the sample A results from uneven particle size of MgO in the refractory.

The molten slag charged in a platinum-rhodium (20mass%) crucible (21mmI.D. $\times$ 10mm in height) in the heating zone of the furnace formed a convex surface above the crucible mouth due to its surface tension. The bottom surface of the rectangular-shaped sample (10_20_100mm in length) was contacted with the slag surface to start the slag penetration. The slag penetration into the sample was directly observed with the X-ray radiographic apparatus and recorded on videotape. After experiments, the sample was removed from the furnace and cooled. Some of the cooled samples were investigated to determine the behavior of the slag penetration. Penetration height of the slag was measured from photographs printed out from the videotape. Experimental conditions were summarized in Table 3.

2.2 Microstructural analysis of the samples after penetration experiments

The cooled sample was cut at the position of 40mm from the bottom surface. The lower part (10_20_40mm in length) was vertically divided into two equal parts paralleling with the 20_40mm surface as analysis samples. Sample A in No.23 experiment (referred to as specimen 23) and sample B in No.24 experiment (referred to as specimen 24) as shown in Table 3 are analyzed. Cross section of the specimen was photographed and analyzed with backscattered electron (BSE) images for the bottom, middle and upper part of the penetrated area. Element mapping of the cross section was carried out for both specimen 23 and 24. BSE images and element mapping of the as-received samples were also performed to compare with the penetrated specimens. Quantitative analysis of the penetrated components with EPMA was carried out for specimen 23.

3 Results

3.1 Behavior of slag penetration into MgO refractory

In-situ observation of slag penetration into MgO refractory was successfully performed with the X-ray radiographic apparatus. Fig.3 shows the image of slag penetration *in-situ* observed with X-ray apparatus. The slag penetration into dense sample C was not observed during the experiment for 10 min. Figs.4~7 show the influences of T.Fe concentration, Al_2O_3 concentration and basicity (C/S ratio) in the slag, and temperature on the rate of slag penetration (variation of penetration height with time). The slag penetrates rapidly into both sample A and B. Under the same experimental conditions, the rate of slag penetration into the sample B is always larger than that into the sample A. The rate of slag penetration into both sample A and B increases with increasing T.Fe concentration in the slag and temperature, and with decreasing the slag basicity. In the case of 10 mass% Al_2O_3-bearing slag, the rate of slag penetration is less than that of Al_2O_3-free slag in the initial stage. The penetration also stops much earlier than that of Al_2O_3-free slag, and then, the penetration height keeps almost constant.

3.2 Microstructure of the refractory after the experiments

Fig.8 shows that the slag penetrated about 25 mm into specimen 23 and about 30 mm into specimen 24. The color of the unpenetrated part in the specimen23 is opaline, and red-brown for the specimen 24. The color of bulk slag phase is dark-brown, which is caused by iron oxide in the slag. Change in color and its distribution shown in Figs.8~12 indicate that the slag penetrates unevenly into the specimen 23 with uneven pore size in a route like a tree, firstly along the main route (the surface of large MgO particles), and then extending to the branch route. However, the slag penetrates evenly into specimen 24 with even pore size.

Figs.9 and 10 are BSE images of specimen 23 and 24, respectively. As shown in Figs.9 and 10, the number of large pores unfilled with slag increases from the middle to the upper part in both specimen 23 and 24. It results from that the slag creeps up along the surface of MgO particles (the surface of the pores) due to the good wettability between the slag and MgO particles, and small pores are filled by the slag in preference to large pores.

Figs.9 and 10 also show that the space among MgO particles in the bottom and middle part of the penetrated area, especially for the specimen 24, is a little larger than that in the as-received part. It can be attributed to the fact that the surface of MgO particle is dissolved by the penetrated slag. It means that the pore size in the penetrated area of the refractory is enlarged during the slag penetration.

3.3 Distribution of the penetrated slag components

Figs. 11 and 12 are the element mappings of specimen 23 and 24. Concentrations of Si, Ca, and Al in the specimen 23 are almost the same from the bottom to the upper part in the penetrated area. Although there is no great difference of Fe concentration among the bottom, middle and upper part in the penetrated area, Fe distribution is not uniform in the whole cross section, which can also be deduced from the color difference in the photographs. Much more Fe is detected in the main route of slag penetration than that in the branch route.

Concentrations of Si, and Ca in the specimen 24 are almost the same in the area from the bottom to the place of 20mm in height, while decrease gradually in the zone of above 20mm from the bottom surface. Fig.12(b) shows that Fe is detected even in the center of MgO particles both in the bottom and in the middle part. The Fe concentration on the surface of MgO particles is very high. Both the Fe content in the MgO particles and the Fe concentration in the penetrated slag decrease from the bottom to the upper part of the penetrated area. Al concentration in the specimen 24 increases gradually from the bottom to the middle part, and reaches the highest in the zone of 10~20mm from the bottom surface. After that, it steeply decreases in the upper part (Al is scarcely detected in the zone of above 20mm from the bottom surface). Al is concentrated on the surface of MgO particles in the specimen 24.

Table 4 shows minerals of the penetrated slag detected in the cooled specimen 23. It indicates that all the minerals detected in the cooled specimen 23 contain MgO.

4 Discussion

4.1 Analysis on the behavior of slag penetration

The slag penetration into porous refractory can be described with a penetration model of liquid into the vertical and cylindrical capillary (referred to as the capillary model), as shown in Fig.13. The rate (variation of penetration height with time) V of the slag penetration into the capillary with the radius r can be expressed as Eq.(1) which is derived from the equations given by E.W.Washburn [3].

$$V = \frac{dh}{dt} = \frac{r^2 \Delta P}{8\eta h} \tag{1}$$

$$\Delta P = \Delta P_c + \Delta P_s \tag{2}$$

where h (m) is the penetration height from the slag surface, ΔP (N/m^2) is the pressure

difference between the two ends of the capillary, ΔP_c (N/m^2) is the capillary pressure, ΔP_s (N/m^2) is the hydrostatic pressure caused by the penetrated slag, η ($N \cdot s/m^2$) is the viscosity of the penetrated slag in the refractory, and t(s) is the penetration time.

The capillary pressure ΔP_c is given by Eq. (3).

$$P_c = \frac{2\sigma \cos\theta}{r} \tag{3}$$

where θ (rad) and σ (N/m) are the surface tension and the contact angle of the slag with the refractory, respectively.

The hydrostatic pressure ΔP_s is given by Eq.(4).

$$\Delta P_s = -\rho g h \tag{4}$$

where ρ (kg/m^3) is the density of the penetrated slag, and g is the gravitational acceleration.

Substituting Eqs. (2)~(4) into Eq.(1), then

$$V = \frac{dh}{dt} = \frac{r^2}{8\eta h}\left(\frac{2\sigma \cos\theta}{r} - \rho g h\right) \tag{5}$$

The hydrostatic pressure ΔP_s may be neglected in comparison with ΔP_c because of $\Delta P_s \ll \Delta P_c$ in the initial stage of penetration. The physicochemical properties of the penetrated slag, such as $\sigma, \theta, \rho, \eta$, are assumed to keep constant in the initial stage of penetration. Then, the relationship between the penetration height and time are obtained as Eqs.(6) and (7) by integrating Eq.(5) from t=0 to t and h=0 to h.

$$h = k_c t^{1/2} \tag{6}$$

$$k_c = \left(\frac{r\sigma \cos\theta}{2\eta}\right)^{1/2} \tag{7}$$

Eqs.(6) and (7) indicate that the rate of slag penetration increases with increasing the radius of the pores and the surface tension of the slag and with decreasing the contact angle ($\theta < \pi/2$ rad) of the slag with the refractory and the slag viscosity. In the initial stage of penetration, the penetration height is proportional to the square root of penetration time ($t^{1/2}$). Based on Eq.(6), the observed penetration height is treated with the least square method and shown in Figs.4~7 as lines and equations.

k_c in Eq.(7) can be regarded as the theoretical penetration coefficient, while the constant in equations of Figs.4~7 is the observed penetration coefficient (k_o). The influences of T.Fe concentration, basicity of the slag and temperature on the rate of slag penetration obtained by experiment can be qualitatively explained with the theoretical penetration coefficient k_c. However, the theoretical penetration coefficient k_c should be different from the observed penetration coefficient k_o because the ideal model process in Fig.13 differs from the actual penetration process in the following points: 1) Actual penetration path in the sample is not straight. It is zigzag. Then, the observed penetration height is smaller than the length of the actual penetration. 2) The pores in samples are not uniform. 3) Composition of the penetrated slag is different from that of the initial bulk slag due to the reaction between the refractory and the penetrated slag, especially in the late stage of the penetration.

As described in 3.1, under the same experimental conditions, the rate of slag penetration into the sample B is always larger than that into the sample A. It is attributed to the fact that the pore size and apparent porosity in the sample B are larger than those in the sample A as shown in Fig.2 and Table 2.

Increasing T.Fe concentration of $CaO\text{-}FeO\text{-}SiO_2$ slag in the concentration range of this research increases the surface tension of the slag and decreases the viscosity of the slag[4], which results in the increase in the rate of slag penetration as predicted from Eq.(6).

In general, increasing temperature lowers the slag viscosity to a great extent, while the change of the surface tension of the slag is a little. So the rate of slag penetration increases with increasing temperature.

Decreasing the slag basicity in the composition range of this experiment remarkably decreases the slag viscosity and slightly decreases the surface tension of the slag[4]. Then, the rate of slag penetration increases with decreasing the slag basicity. For example, in the case of the slags (T.Fe=30mass%) with the basicity of 1, 2 and 3 at 1673K, the values of viscosity are 0.05, 0.2 and 1.2N·s/m^2 (extrapolated), and the values of surface tension are 0.51, 0.55 and 0.60N/m (extrapolated), respectively[4]. The calculated values from the theoretical penetration coefficient k_c for the slags with the basicity of 1, 2 and 3 are 17.2, 8.9 and 3.8 mm/s$^{1/2}$ for the sample B, and 12.1, 6.2 and 2.7 mm/s$^{1/2}$ for the sample A, respectively, by assuming that the contact angle of the CaO-FeO-SiO_2 slag with MgO refractory is 0 rad and the pore radius of sample B and A is 50 μm and 25 μm, respectively. The above theoretical analysis confirms that the rate of slag penetration increases with decreasing the slag basicity and the rate of slag penetration into the sample B is larger than that into the sample A under the same conditions because of the larger pore size in the sample B than that in the sample A.

In addition, decreasing the slag basicity increases the solubility of MgO in the slag[5], Therefore, it can increase the radii of the pores due to the dissolution of MgO from refractory into the penetrated slag. It may also results in the increase in the rate of slag penetration predicted from Eq.(6).

The influence of Al_2O_3 in the slag on the behavior of slag penetration is explained in 4.2.

4.2 Behaviors of the penetrated slag components

The penetrated slag dissolves MgO particles, which is verified by the fact that all the minerals in the penetrated slag detected in the cooled specimen contain MgO (Table 4).

Fe_tO in the penetrated slag is absorbed into MgO particles and forms solid solution with MgO, resulting in the decrease of the Fe_tO concentration in the penetrated slag. As shown in Figs.11 and 12(a), Much more Fe is detected in the main route than that in the branch route for the specimen 23, which indicates that Fe_tO is firstly consumed in the main route by the absorption and then it is further consumed in the branch route. In the case of specimen 24, the color difference appears in the vertical direction of the penetrated slag area. Fe_tO concentration in the penetrated slag decreases gradually from the bottom to the upper part with the absorption of Fe_tO by the MgO particles. The Fe_tO content in the MgO particles also decreases due to the decrease of the Fe_tO concentration in the penetrated slag. The decrease of Fe_tO concentration in the penetrated slag causes the increase in the melting point as well as the increase of viscosity and the decrease of surface tension as mentioned in 4.1. For example, for the CaO-FeO-SiO_2 (C/S=1.0) slag, the melting point increases from 1473K to 1673K when the T.Fe concentration in the penetrated slag decreases from 25 mass% to 11 mass%[6].

Al_2O_3 in the penetrated slag reacts with MgO refractory, and forms spinel on the pore surface (at the boundary between the penetrated slag and the surface of MgO particles), which is verified by the fact that Al is concentrated on the surface of MgO particles as shown in Fig.12. Al_2O_3 concentration in the penetrated slag decreases during its penetration due to the formation of the spinel. In the case of specimen 24, Al_2O_3 in the penetrated slag is almost consumed when the slag penetrates into the middle part. About 8% volume expansion occurs due to the formation of the spinel[7]. The pore size can be reduced by the formation and accumulation of the spinel on the pore surface and also by the volume expansion of the spinel. The decrease of the pore diameter suppresses the further penetration of the slag. Therefore, the penetration of the 10mass% Al_2O_3-bearing slag stops much earlier than that of Al_2O_3-free slag.

Thus, the slag penetration is deduced to stop due to the followings: 1) The melting point and viscosity of the penetrated slag increase, and the surface tension of the penetrated slag

decreases with decreasing the Fe_tO concentration in the penetrated slag consumed by the reaction between Fe_tO and MgO particles. 2) In the 10mass%Al_2O_3-bearing slag, the pore size in the refractory can be reduced by the spinel formed on the pore surface by the reaction between Al_2O_3 in the penetrated slag and MgO particles in the refractory.

5. Conclusions

In-situ observation of slag penetration into MgO refractory was successfully conducted with the X-ray radiographic technique. Based on *in-situ* X-ray observation and microstructural analysis of the samples after penetration experiments, the following results were obtained.

The slag penetrates rapidly into the refractory, reacting with MgO particles in the refractory. The slag penetrates unevenly into the refractory with uneven pore size in a route like a tree, firstly along the main route (the surface of large MgO particles), and then extending to the branch route, while it penetrates evenly into the refractory with even pore size.

The rate of slag penetration increases with increasing pore radius and apparent porosity of the refractory, T.Fe concentration in the slag and temperature, and with decreasing the slag basicity. In the case of the Al_2O_3-bearing slag, the rate of slag penetration is less than that of Al_2O_3-free slag in the initial stage. The penetration also stops much earlier than that of the Al_2O_3-free slag, and then the penetration height keeps almost constant.

In the initial stage of slag penetration, the penetration height is proportional to the square root of the penetration time, and the penetration behaviors of the slag can be qualitatively explained with the model derived from the equations given be E.D.Washburn[3].

Slag penetration is deduced to stop due to the followings: 1) The melting point and viscosity of the penetrated slag increase, and the surface tension of the penetrated slag decreases with decreasing the Fe_tO concentration in the penetrated slag consumed by the reaction between Fe_tO and MgO particles. 2) In the 10mass%Al_2O_3-bearing slag, the pore size in the refractory is reduced by the spinel formed on the pore surface due to the reaction between Al_2O_3 in the penetrated slag and MgO particles in the refractory.

References

1) Goto, K., Argent, B. B. and Lee, W. E.: Corrosion of MgO-$MgAl_2O_4$ spinel refractory bricks by calcium aluminosilicate slag. J. Am. Ceram. Soc., 80(2) 461-471(1997).
2) Z.Yu, K.Mukai, K. Kawasaki and I. Furusato: Relation between corrosion rate of magnesia refractories by molten slag and penetration rate of slag into refractories. J. Am. Ceram. Soc. Japan, 1010(5) 533-539 (1993)
3) E.D.Washburn: The dynamicx of capillary flow. Phys. Rev.,XVII(1921), 273~283.
4) The committee for fundamental metallurgy: Slag atlas. Germany, 1981.
5) J.Bygden, T.DebRoy and S. Seetharaman: Dissolution of MgO in stagnant CaO-Fe_tO-SiO_2 slags. Ironmaking and Steelmaking. 1994, Vol.21, NO.4, 318~323.
6) Ernest M. Levin, et al.: Phase diagram for ceramists, USA. 1961.
7) M. Ezoe: Properties and application of spinel for refractory. TAIKABUTSU, 43(1) (1991), 29-37.

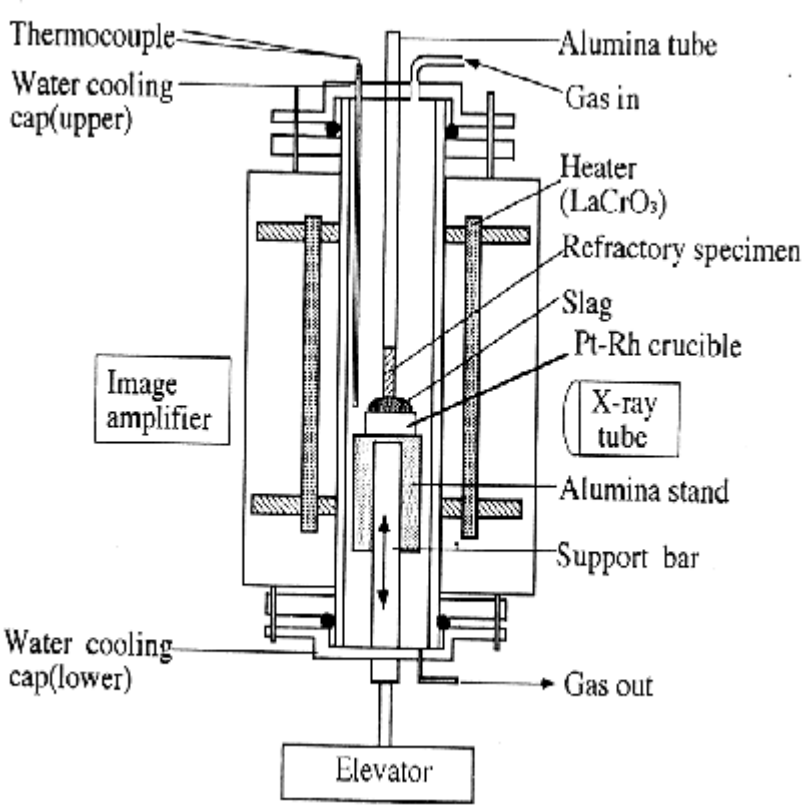

Fig.1 Schematic diagram of the experimental apparatus.

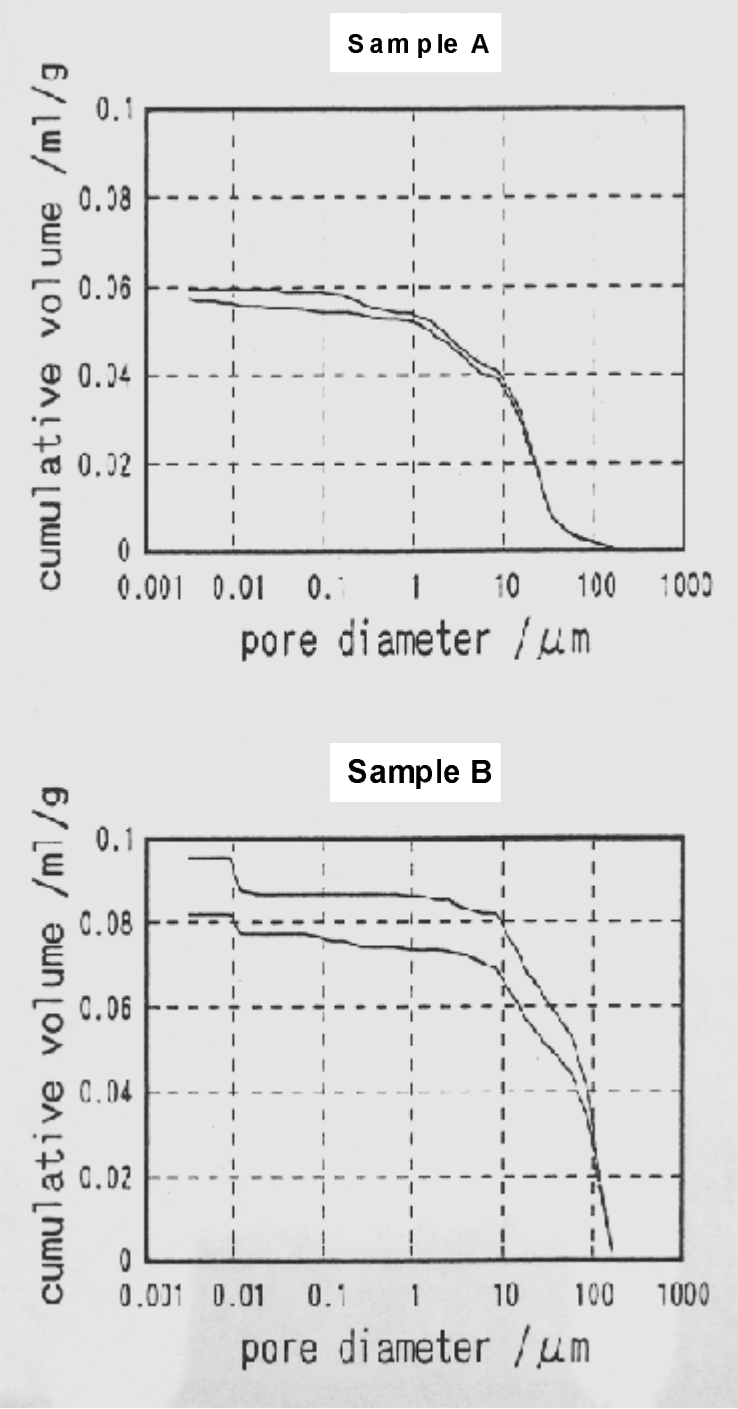

Fig.2 Pore size distribution in the sample A and B.

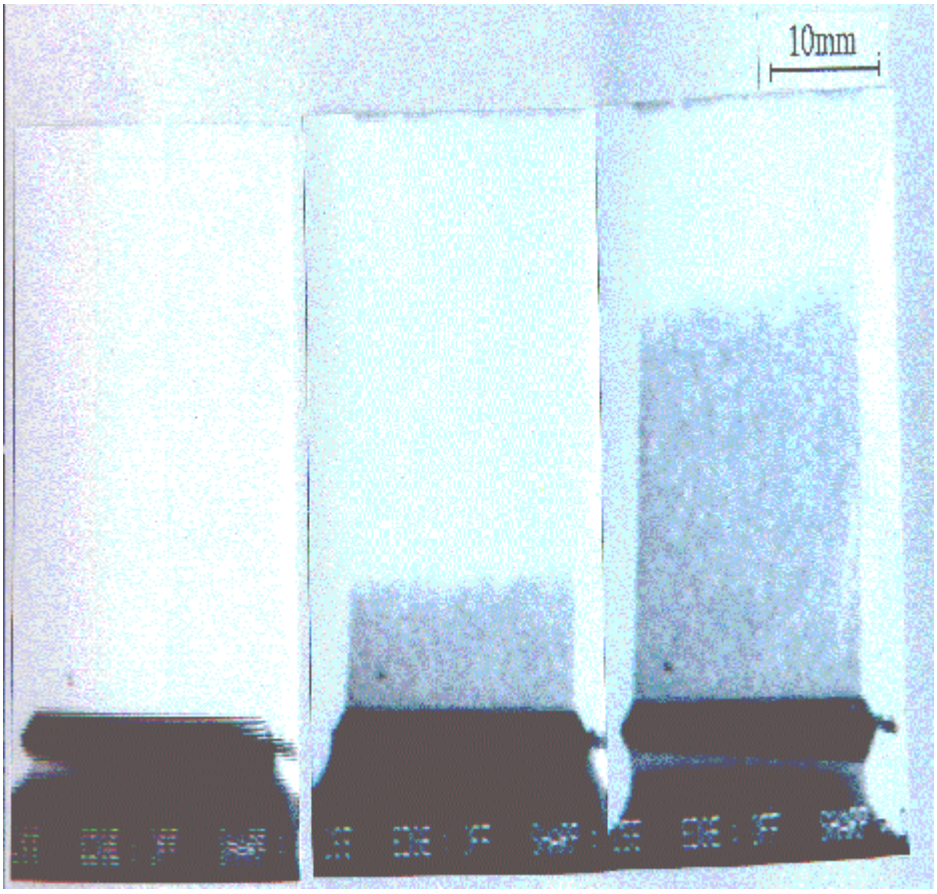

0s 2s 12s

Fig.3 Direct observation of slag penetration into MgO refractory with X-ray transmission device. Porosity of the refractory: 31%. Slag: C/S=2.0, T.Fe=30.0mass%, MgO=5.0mass%. Temperature: 1520℃.

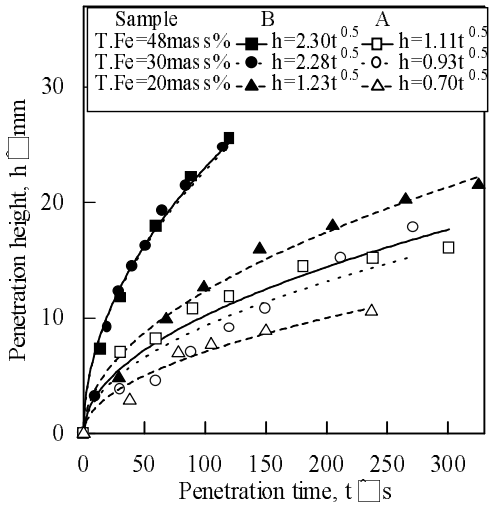

Fig.4 Relationship between penetration height and penetration time with the slag of C/S=1.0, T.Fe=20, 30, 48mass% at 1593K.

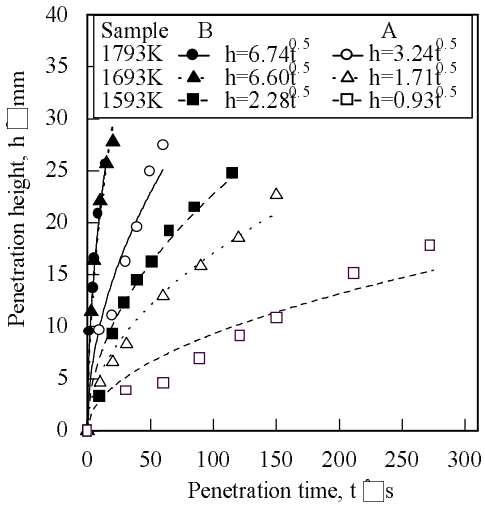

Fig.5 Relationship between penetration height and penetration time with the slag of C/S=1.0, T.Fe=30mass% at 1593K, 1693K and 1793K.

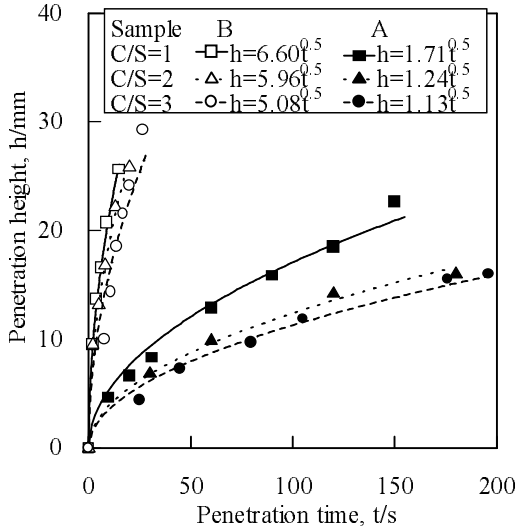

Fig.6 Relationship between penetration height and penetration time with the slag of C/S=1.0, 2.0, 3.0 and T.Fe=30mass% at 1693K.

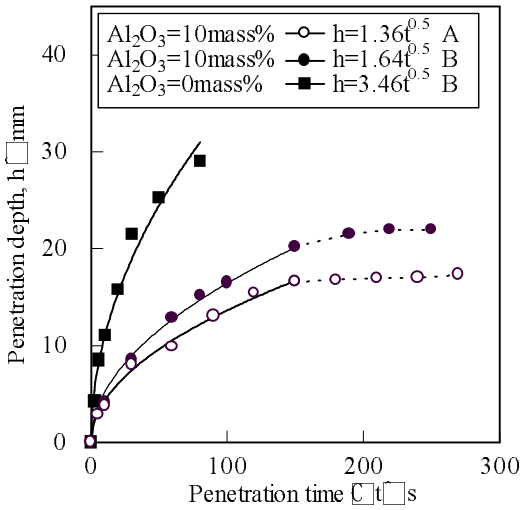

Fig.7 Influence of Al_2O_3 content in the slag (C/S=1.0, T.Fe=25mass%) on the penetration rate of slag at 1593K.

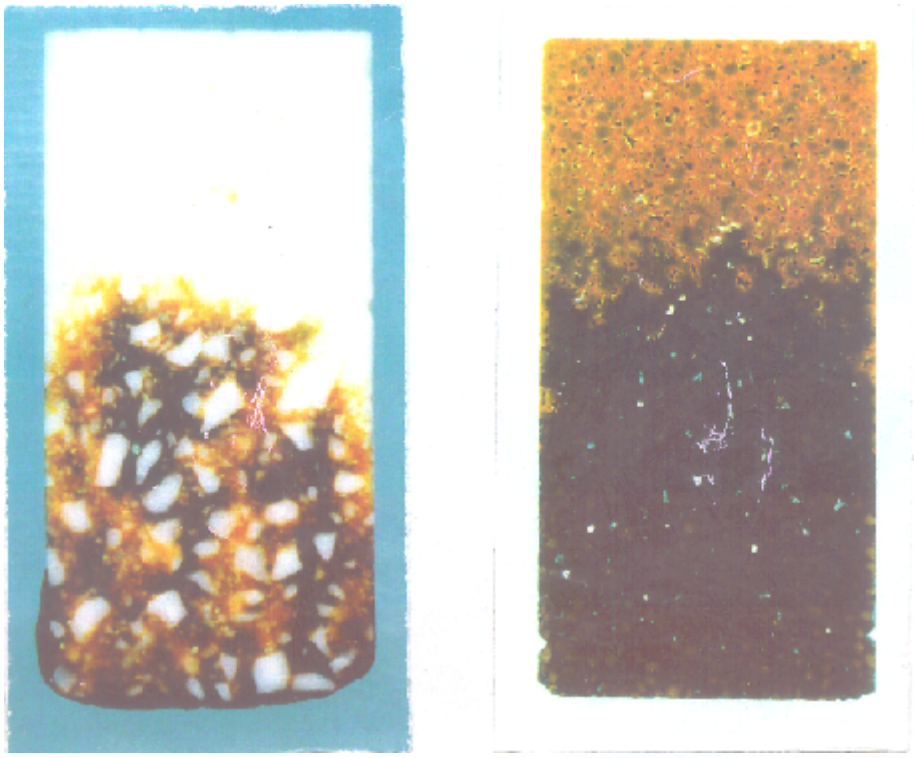

23 24

Fig.8 Cut section of specimens 23 and 24.
Width of the specimens is 20mm.

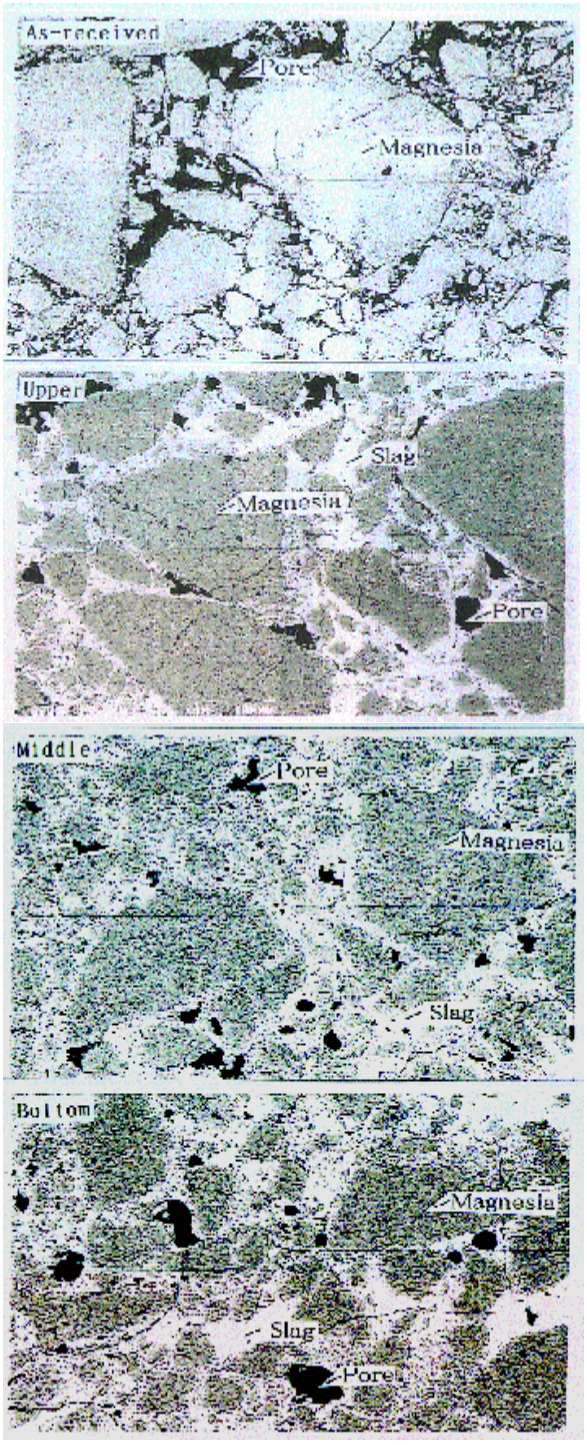

Fig.9 Backscattered electron image of the specimen 23 after the test. O: Original; U: Upper; M: Middle; B: Bottom.

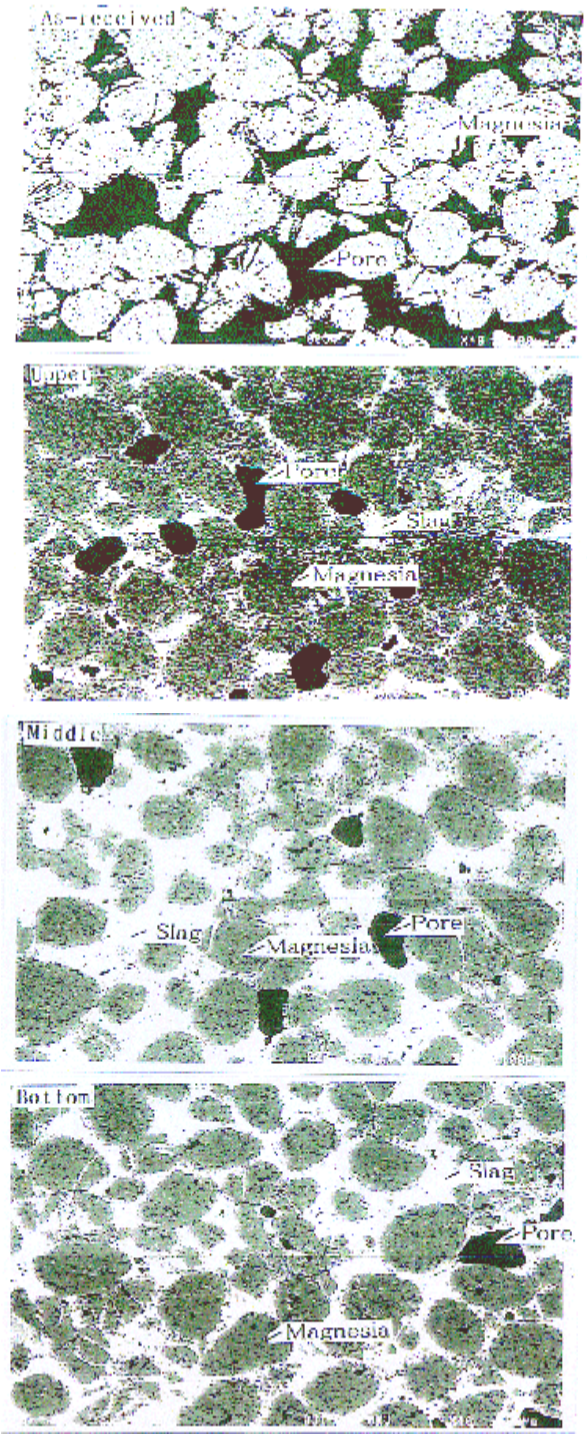

Fig.10 Backscattered electron image of the specimen 24 after the test. O: Original; U: Upper; M: Middle; B: Bottom.

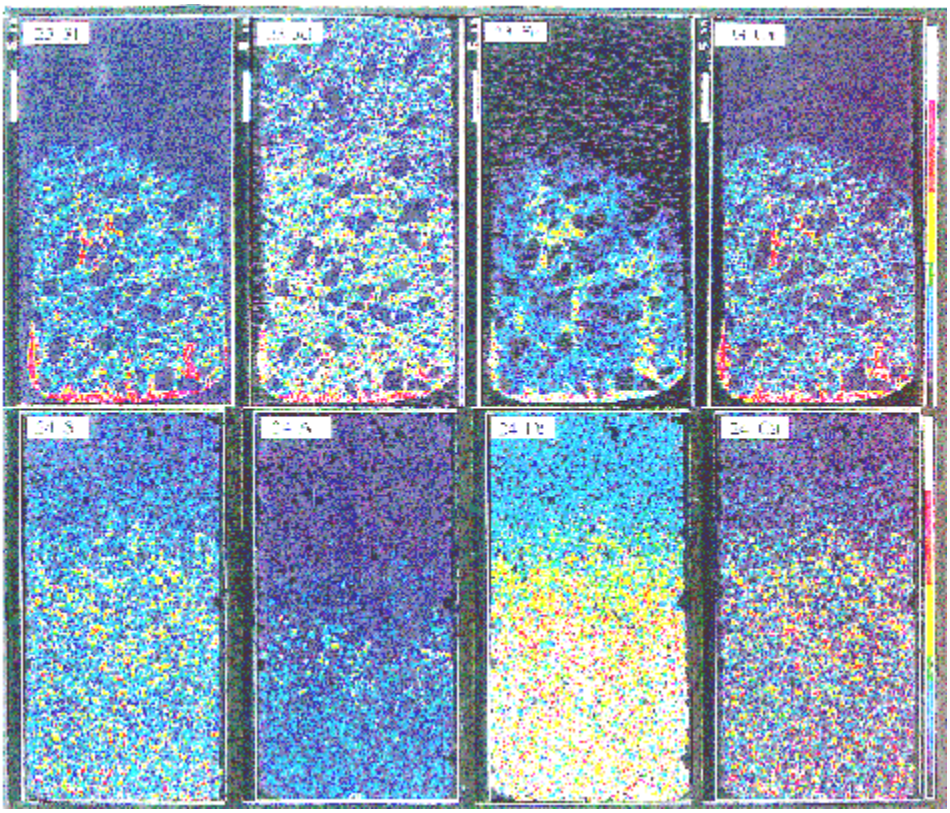

Fig.11 Distribution of Si, Al, Fe and Ca in the specimens 23 and 24 after the test mapped by EPMA.

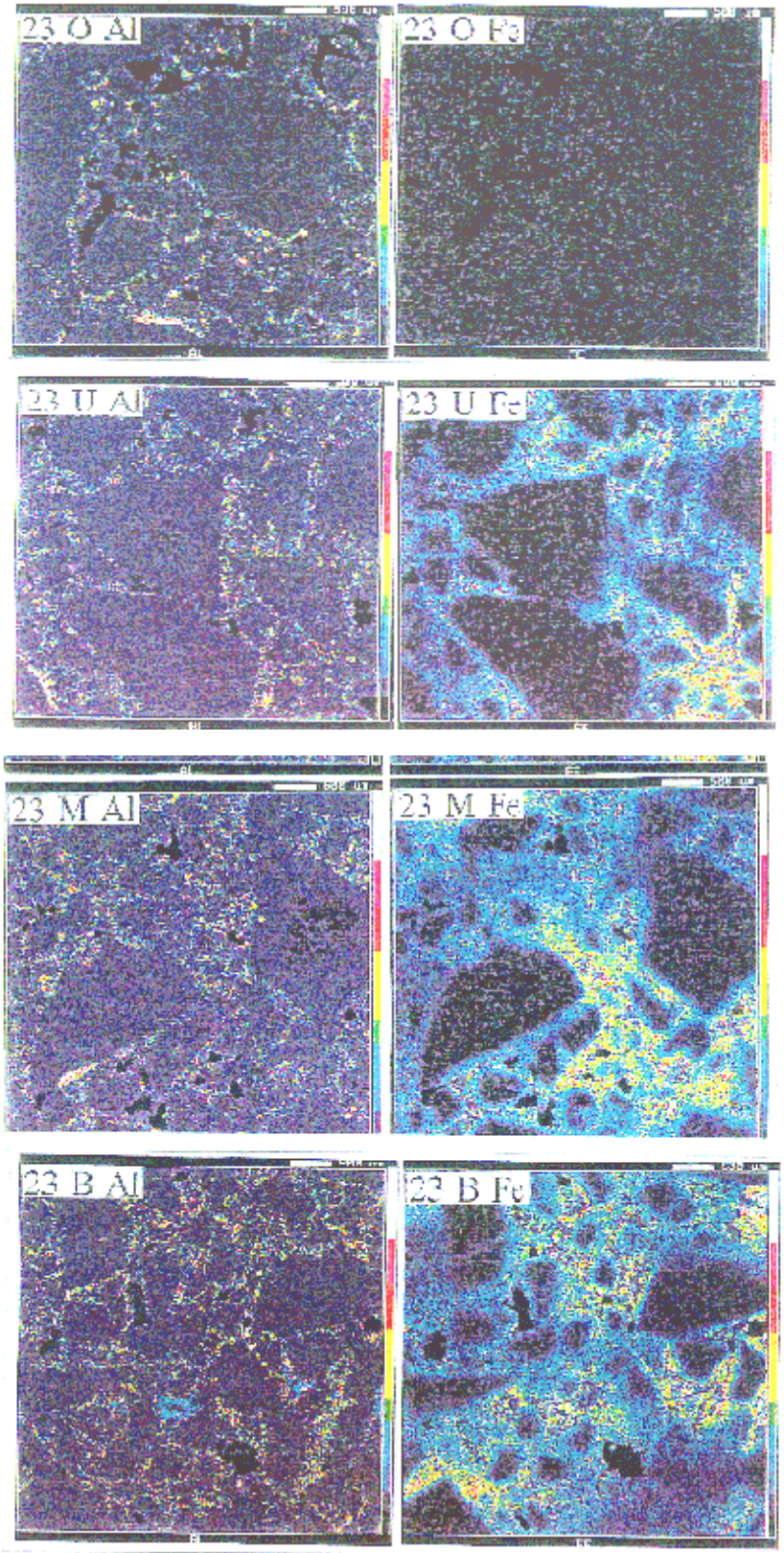

Fig.12(a) Distribution of Al and Fe in the specimen 23 after the test mapped by EPMA. O: Original; U: Upper; M: Middle; B: Bottom.

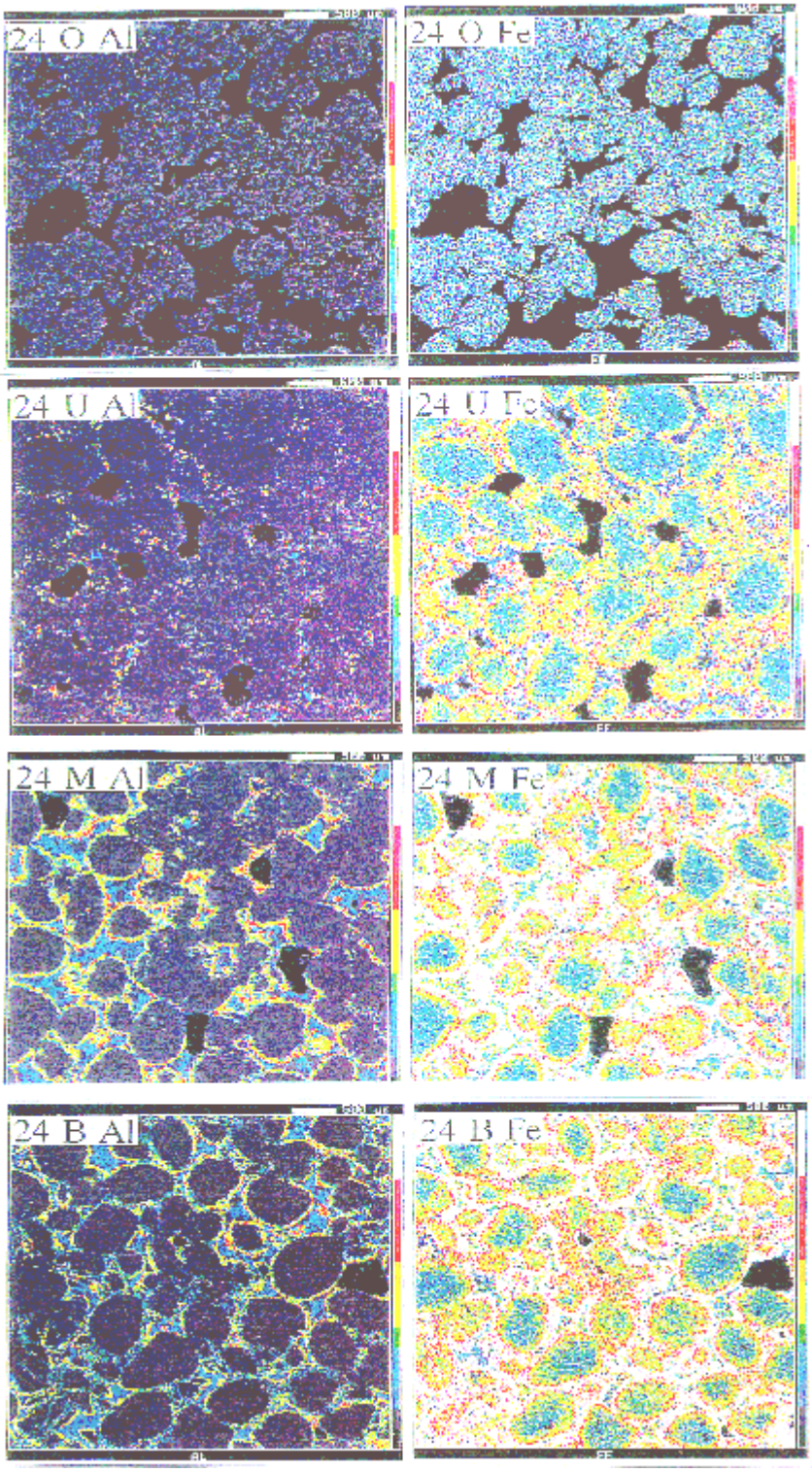

Fig.12(b) Distribution of Al and Fe in the specimen 24 after the test mapped by EPMA. O: Original; U: Upper; M: Middle; B: Bottom.

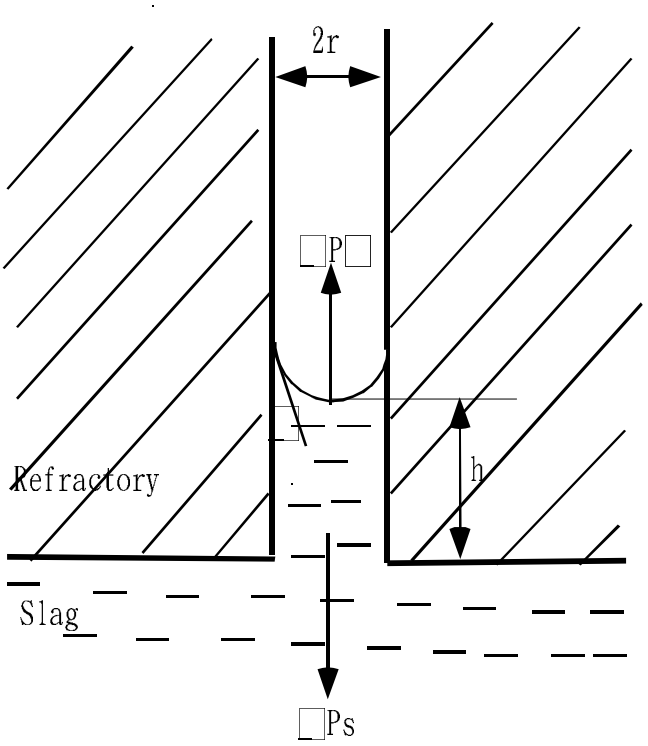

Fig.13 Model for slag penetration into capillary.

Table 1 Slag composition (mass%).

No.	No.1	No.2	No.3	No.4	No.5	No.6	No.9
SiO_2	37.0	30.8	19.0	20.5	15.4	28.7	33.9
Al_2O_3	–	–	–	–	–	10.0	–
T.Fe※	20.0	30.0	48.0	30.0	30.0	25.0	25.0
CaO	37.0	30.8	19.0	41.0	46.2	28.7	33.9
MgO	–	–	–	–	–	–	-
C/S	1.0	1.0	1.0	2.0	3.0	1.0	1.0

※ Total amount of iron shown in the metal form.

Table 2 Properties of magnesia refractories used in the experiments.

Sample	A	B	C
Chemical composition(mass%)			
SiO_2	0.12	3.79	-
Al_2O_3	1.93	0.44	-
Fe_2O_3	0.01	0.00	-
FeO	0.27	2.03	-
CaO	0.92	1.12	-
MgO	95.57	94.95	99.9
Apparent specific density	2.88	2.42	3.44
Apparent porosity (%)	17.7	31	0.3
Cold crushing strength (MPa)	49	18.0	-
Cold bending strength (MPa)	-	9.2	-
Manufacturer	Kurosaki	Kurosaki	Nikkato

Table 3 Experimental conditions.

Experiment	Sample	Slag(mass%)					Temperature(K)	Atmosphere
		No.	C/S	Al_2O_3	T.Fe	MgO		
1	B	No.1	1.0	-	20.0	-	1593	Ar
2	A	No.1	1.0	-	20.0	-	1593	Ar
4	B	No.3	1.0	-	48.0	-	1593	Ar
5	A	No.3	1.0	-	48.0	-	1593	Ar
6	A	No.2	1.0	-	30.0	-	1593	Ar
7	A	No.2	1.0	-	30.0	-	1693	Ar
8	A	No.2	1.0	-	30.0	-	1793	Ar
9	B	No.2	1.0	-	30.0	-	1593	Ar
10	B	No.2	1.0	-	30.0	-	1793	Ar
11	B	No.2	1.0	-	30.0	-	1693	Ar
12	A	No.4	2.0	-	30.0	-	1693	Ar
13	B	No.4	2.0	-	30.0	-	1693	Ar
14	A	No.5	3.0	-	30.0	-	1693	Ar
15	B	No.5	3.0	-	30.0	-	1693	Ar
23	A	No.6	1.0	10.0	25.0	-	1593	Ar
24	B	No.6	1.0	10.0	25.0	-	1593	Ar

Table 4 Minerals detected in the specimen 23.

Area	Upper	Middle	Bottom
Monticellite ($CaMgSiO_4$)	○	○	○
Merwinite ($Ca_3MgSi_2O_8$)	○	○	○
Fe-bearing spinel $(Mg(Al,Fe)_2O_4$	○	○	○
Melilite solid solution*	?		○

*Gehlenite($Ca_2SiAl_2O_7$)-akermanite($Ca_2MgSi_2O_7$) solid solution.
Upper: highest part of the penetrated area (above 20mm).
Middle: middle part of the penetrated area (about 10~20mm).
Bottom: bottom part of the penetrated area (about 0~10mm).